World Academy of Science, Engineering and Technology
International Journal of Mechanical and Mechatronics Engineering
Vol:18, No:4, 2024

Study of the Effect of Rotation on the Deformation of a Flexible Blade Rotor

Aref Maalej, Marwa Fakhfakh, Wael Ben Amira

Abstract**—**We present in this work a numerical investigation of fluid-structure interaction to study the elastic behavior of flexible rotors. The principal aim is to provide the effect of the aero/hydrodynamic parameters on the bending deformation of flexible rotors. This study is accomplished using the strong two-way fluid-structure interaction (FSI) developed by the ANSYS Workbench software. This method is used for coupling the fluid solver to the transient structural solver to study the elastic behavior of flexible rotors in water. In this study, we use a moderately flexible rotor modeled by a single blade with simplified rectangular geometry. In this work, we focus on the effect of the rotational frequency on the flapwise bending deformation. It is demonstrated that the blade deforms in the downstream direction and the amplitude of these deformations increases with the rotational frequencies. Also, from a critical frequency, the blade begins to deform in the upstream direction.

Keywords**—**Numerical simulation, flexible blade, fluid-structure interaction, ANSYS Workbench, flapwise deformation.

I. Introduction

ROTORS play a crucial role in numerous engineering and everyday life applications, particularly in electric generators like wind and hydrokinetic turbines, as well as in flying objects such as helicopters, drones, and airplanes. Over the past decades, research has been focused on developing reliable and efficient large-scale wind turbines in response to the increasing demand for energy. This has led to the use of increasingly high-performance materials, with most wind turbine blades now made from composite materials that combine lightness and strength [1].

However, the enlargement of rotor size and the use of lightweight materials introduce deformations in the blades, which disrupt the flow around the rotors and affect their performance. Therefore, studying the aerodynamic problems associated with elasticity has become important. Previous studies have investigated the effect of structural flexibility on the performance of flapping wings [2] and the reduction of drag through flexibility and reconfiguration [3], [4]. However, these studies have primarily focused on the impact of flow velocity on aerodynamic performance.

To gain a deeper understanding of aeroelasticity, numerous studies have been presented. The main goals of these studies are to improve the performance of wind turbines by increasing their efficiency and energy production, characterizing the aerodynamic parameters and blade aspects [5], studying and characterizing the flow and stability of the wake behind the rotors [6], and predicting the aerodynamic loads on the blades [7]-[9]. These efforts contribute to advancing wind turbine technology and its integration into sustainable power generation.

Aref Maalej, Marwa Fakhfakh, and Wael Ben Amira are with University of Sfax, National School of Engineers of Sfax, Laboratory of Electromechanical Systems (LASEM), Sfax, Tunisia (e-mail: aref.maalej@enis.tn).

II. Governing Equations

FSI problems for a transient structure in turbulent flow are modeled by the incompressible Navier-Stokes equations and the linear equations of elasticity. These phenomena are described by the following systems:

$$\rho_f \frac{\partial \boldsymbol{u}_f}{\partial t} + \rho_f(\boldsymbol{u}_f.\nabla)\boldsymbol{u}_f = -\nabla p + \mu_f \nabla.(\nabla \boldsymbol{u}_f) + F_v$$

$$\nabla.\boldsymbol{u}_f = 0 \tag{1}$$

$$\rho_s \frac{\partial \boldsymbol{u}_s}{\partial t^2} - \nabla.\sigma^{solid} = F_s \tag{2}$$

where $\mathbf{u}_f$ is the incompressible fluid velocity field, $\mathbf{u}_s$ is the displacement of the solid blade, t is the time, μ_f is the dynamic viscosity, F_v is the body force on the fluid, in this case gravitational acceleration times ρ_f, and F_s is the force per unit volume on the blade. ρ_f and ρ_s are the fluid's and solid's density, respectively.

$$\sigma^{solid} = 2\mu_s \varepsilon + \lambda_s tr(\varepsilon)\boldsymbol{I} \tag{3}$$

with:

$$\mu_s = \frac{E}{2(1+\upsilon)} \quad \text{and} \quad \lambda_s = \frac{E\upsilon}{(1+\upsilon)(1-2\upsilon)} \tag{4}$$

where σ^{solid} is the stress fields, ε is the solid deformation, E is the Young's modulus, ν is the Poisson coefficient, and **I** is the identity tensor.

The coupling equations are modeled by a kinematic condition and a dynamic condition:

$$\boldsymbol{u}_f(x,t) = \frac{\partial \boldsymbol{u}_s}{\partial t} \tag{5}$$

$$\boldsymbol{n}.\sigma^{solid}_{interface} = \boldsymbol{n}.\sigma^{fluid}_{interface} \tag{6}$$

n is the unit per vector normal to the blade; σ^{fluid} is the stress field in the fluid given by:

$$\sigma^{fluid} = -pI + \mu_f(\nabla \boldsymbol{u}_f + (\nabla \boldsymbol{u}_f)^t) \tag{7}$$

III. Numerical Simulation

A. Computational Fluid Dynamics Model

The numerical simulation is performed using the ANSYS Workbench software, employing three modules: one for the numerical modeling of fluid dynamics, a second one for solving the transient structure, and a third one to ensure the coupling between these two.

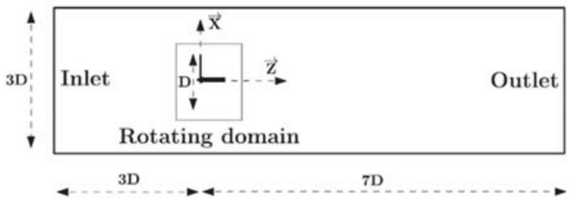

Fig. 1 Computational domain

The fluid domain consists of two subdomains: a stationary rectangular domain representing the flow channel, and a rotating cylindrical domain to characterize the rotor rotation. The dimensions of the computational domain (Fig. 1) are chosen based on numerical requirements and solution convergence.

The stationary domain has dimensions of 38 cm (2.6D) width, 52.8 cm (3D) height and 176 cm (10D) length. The cylindrical rotational domain uses a diameter of 27 cm (1.53D) and width 50 cm (2.84D) to enclose the rotor (blade, hub and shaft). In the previous expressions, D corresponds to the rotor diameter. The domain reference (x,y,z) = (0,0,0) is set at the center of the turbine hub. The origin location of the inlet boundary is at a distance of 3D from the blade and the outlet boundary is 7D from the rotor center.

The simulation is analyzed by the K- Ɛ model. The inlet water flow is defined by a constant velocity of 18 cm/s. The outlet of the flow channel is defined as a zero pressure outlet. The boundary condition of the wall is defined as no-slip and assigned to the different limits of the flow channel as well as to the wall-cfd-coupled (blade, hub and shaft) is defined by the no-slip condition for the velocity to be immediately zero next to the wall.

B. Transient Structure Model

The studied rotor has a radius of R = 88 mm. It consists of a single blade, a hub, and a shaft. The shaft is a 15 mm diameter nylon axis. The hub is made of carbon fiber. The blade is a rectangular airfoil with a constant chord length of c = 20 mm and a uniform thickness of 0.7 mm. It is made of flexible low-density polyethylene (LDPE) with a Young's modulus of 3.5 GPa, a density of 1070 kg/m^3, and a shear modulus of 2.1 GPa. The dimensions of the rotor are summarized in Fig. 2.

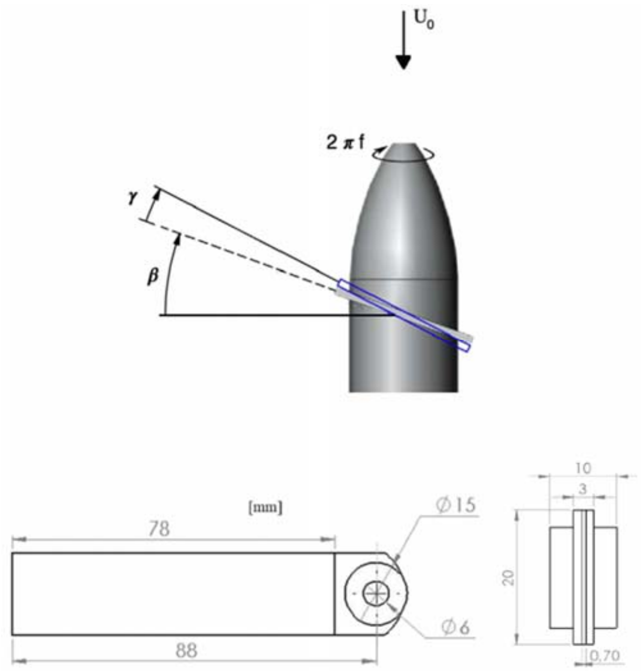

Fig. 2 Rotor, blade, and hub's dimensions

C. Coupled Fluid Structure Interaction Model

The coupling between the fluid domain and the transient structural domain is performed through coupled simulations with bidirectional data transfer.

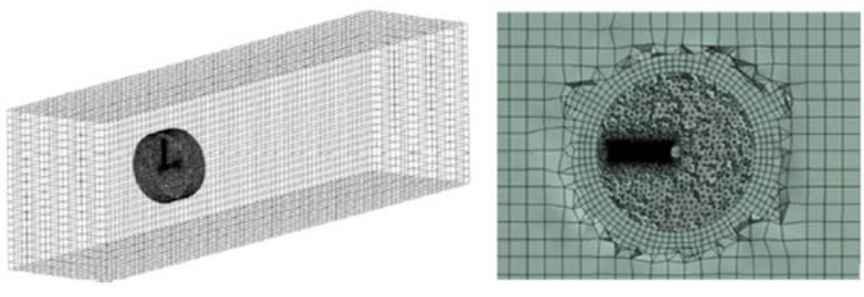

Fig. 3 Grid and sectional view of the computational domain

IV. Meshing

The fluid domain is meshed and divided into a finite number of control volumes, where the conservation equations for continuity and momentum are solved. The computational domain mesh is generated using "Ansys-Meshing." We tested various structured and unstructured meshes to select an optimal mesh that provides good results and reasonable computation time. We achieved a compromise with a mesh consisting of 454188 nodes and 235001 elements (Fig. 3).

Since it is not possible to apply a structured mesh to a 3D dynamic mesh domain [9]-[11], we utilized an unstructured tetrahedral mesh around the blade, particularly in the rotating domain. However, a structured mesh was chosen for the remaining stationary fluid domain. The coupling is ensured by the dynamic meshing at the fluid-structure interface.

The structure domain was discretized using an unstructured tetrahedral mesh. It consisted of 277070 nodes and 137950 elements, distributed as follows: the element size was set to 0.001 m in the blade region to accurately capture deformations, while a larger element size of 0.003 m was used for the rotor and shaft (Fig. 4).

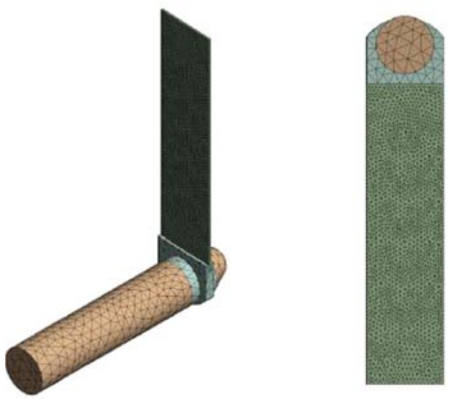

Fig. 4 Structure of the mesh

To account for the turbulence of the flow, the Navier-Stokes equations are augmented with one of the turbulence models (the k-ε model in our case).

V. Results and Discussions

A. Rotational Frequency Effect

In this section, we analyze the bending behavior of the rotor blade and present the effect of the rotation frequency on this kind of deformation for a blade with a pitch angle $\beta = 0°$.

For the present study, the inlet velocity is constant U_0 = 18 cm/s, and the rotor rotation frequency was varied between 0 Hz and 8 Hz which corresponds to tip speed ratios (TSR) $0 < \lambda < 25$, and giving blade tip Reynolds numbers $0 < Re < 0\text{-}8.8 \times 104$.

The total simulation time is 3 s for a step of 1 ms for frequencies below 5 Hz. For higher frequencies, we decrease the time step for convergence conditions.

Fig. 5 illustrates the maximum displacement (over time) and the corresponding stress of the rotor blade at various rotation speeds, considering a blade with a pitch angle of $\beta = 0°$. To simplify the presentation, the rotational speed is expressed in terms of frequency (f).

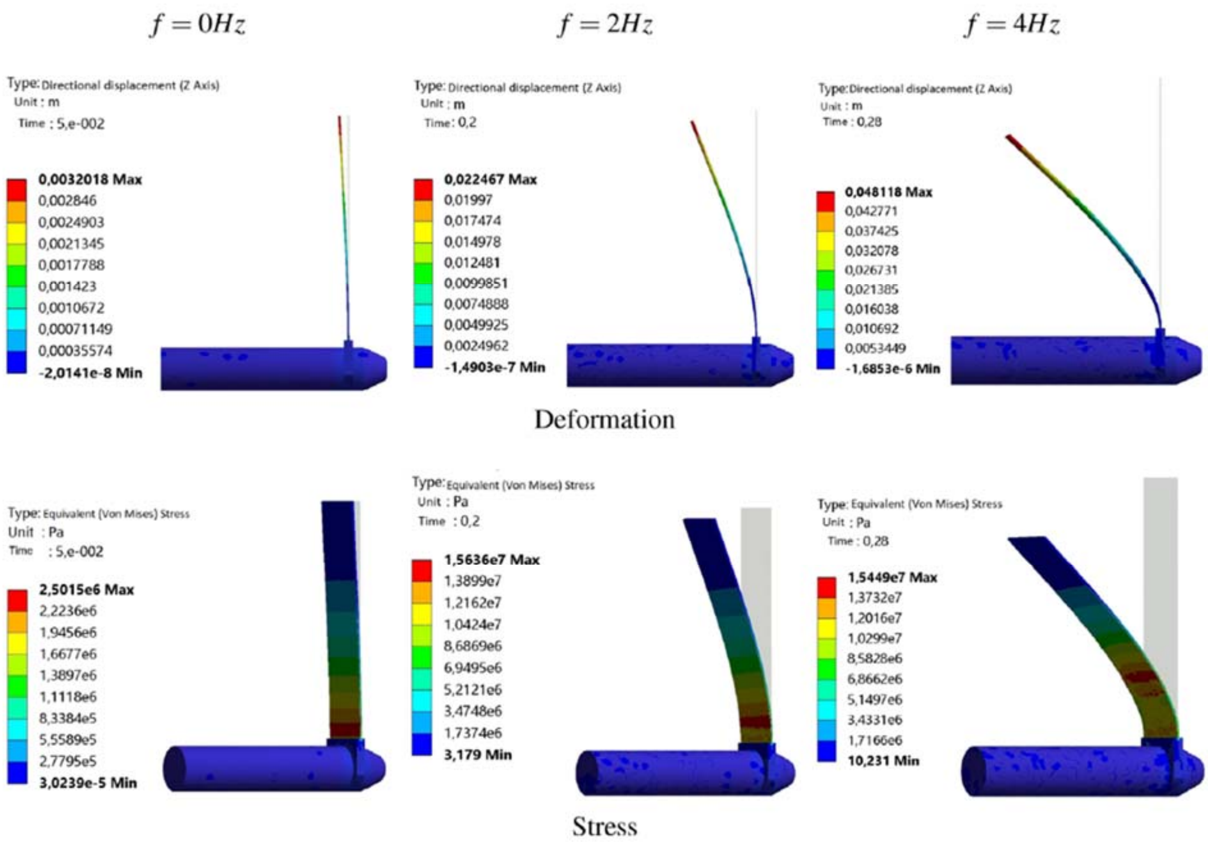

Fig. 5 Maximum flapwise displacement and stress distribution of the blade with β = 0˚, as a function of the rotational frequency f

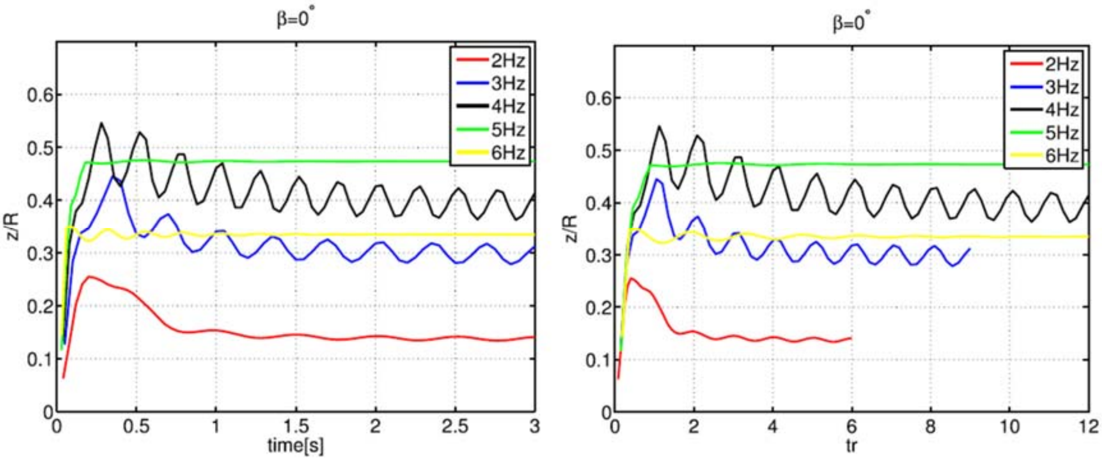

Fig. 6 Total maximum blade deformation variation (a) with time and (b) with number of revolution for different frequencies

The displacement graphs demonstrate that the blade deforms in the downstream direction, and the magnitude of deformation amplifies with increasing rotation frequency. At f = 0 Hz, indicating a non-rotating rotor, the blade remains nearly straight with a slight curvature due to the presence of a non-zero free stream.

In Fig. 6 (a), the temporal evolution of blade deformation (in the z-direction) is depicted for various rotational frequencies. The deformation undergoes a transient phase before stabilizing around an average value after several revolutions. The amplitude of the deformation oscillates with a period corresponding to the blade's rotation frequency.

The deformation vs. time variation for different positive rotation frequencies (Fig. 6) reveals an increase in deformation amplitude with frequency for values below. 5. However, beyond this threshold, the amplitude of deformation starts to decrease.

In conclusion, the bending of the rotor is not a monotonic function with respect to the rotation frequency.

B. Pitch Angle Effect

The pitch angle is an important parameter in controlling the performance of wind turbines. We present, in this section, the effect of this parameter on the blade deformation. Fig. 7 describes the elastic behavior of the blade for different pitch angles and different frequencies.

The displacement figures (Fig. 5) show that the blade deforms in the downstream direction, and the amplitude of the deformation increases with the rotation frequency.

We found that the blade with pitch angle β = 5˚and β = 10˚, for a higher frequency and for a specific instant, begins to deform in the upstream direction. To properly characterize and study this behavior, we present in Figs. 8-10, the evolution of the blade tip displacement with time for different pitch angles and different speed frequencies. The blade with pitch angle β = 5˚, rotating with f = 7 Hz, begins to deform in the upstream direction after nine revolutions. The same blade, rotating with f = 8 Hz, deforms in the upstream direction from the 6th revolution (Fig. 9).

We have found the same behavior for negative frequencies (negative pitch angle), i.e., the deformation increases with rotation frequency except that the amplitude for negative frequencies is greater than that for positive ones (Figs. 8 and 9).

Fig. 11 shows the deformation in the z direction for different pitch angles with a rotational frequency f = 4 Hz. It is clear that the amplitude of the deformation decreases with the pitch angle, due to the orientation of the blade with respect to the flow. Indeed, the quadratic bending moment along the z axis increases and the perpendicular surface to the flow decreases.

VI. Conclusion

We have studied the elastic behavior of moderately flexible rotor. For this study, we used the FSI approach solved numerically with the modules of Ansys workbench software. The coupling between transient structure and fluid dynamics, allowed us to study the effect of the flow on the elastic behavior of the blades. In particular, the effect of rotation frequency on the amplitude of blade deformation.

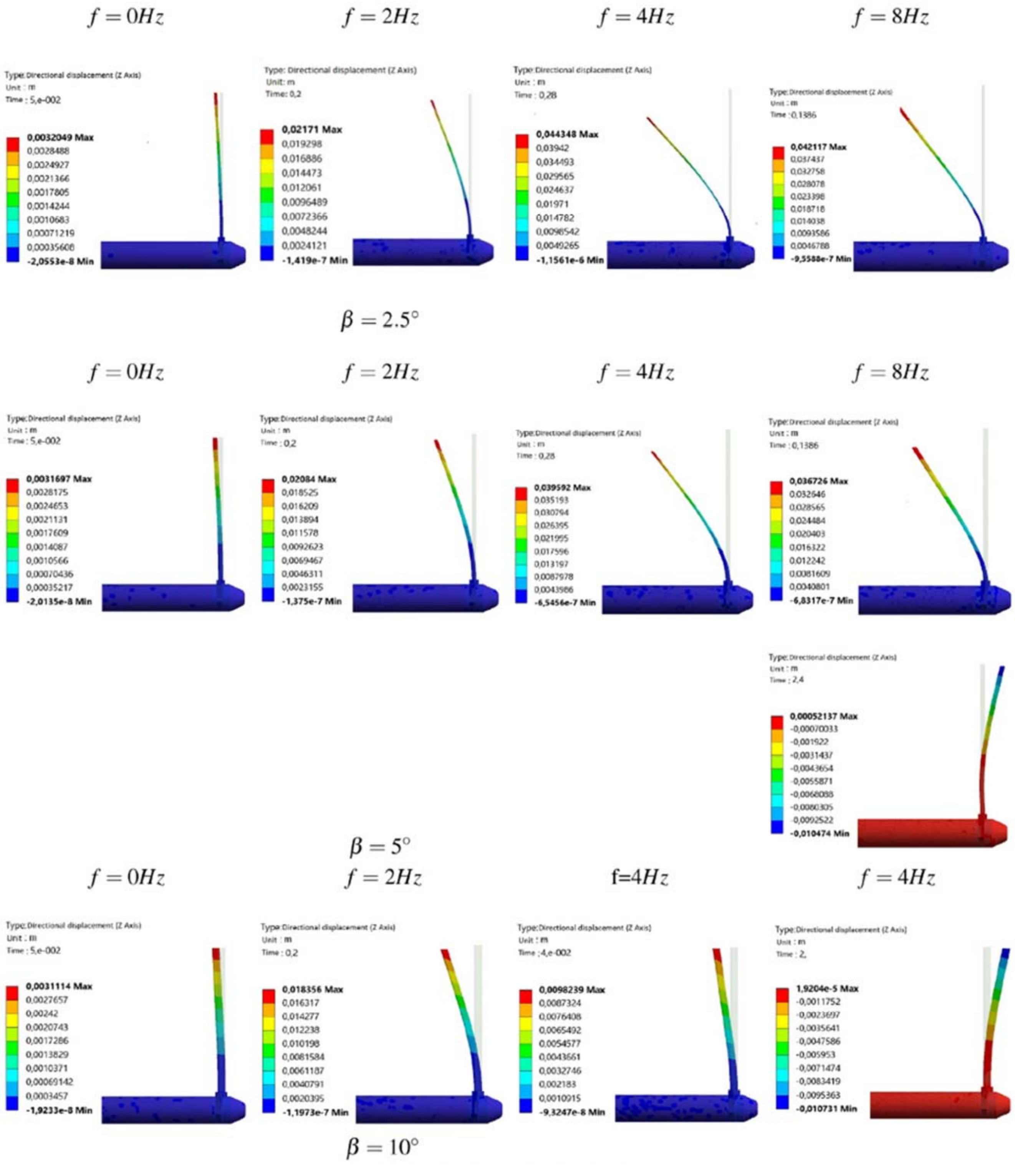

Fig. 7 Maximum flapwise displacement of the blade with β = 2.5˚; β = 5˚ and β = 10˚ as a function of rotational frequency f

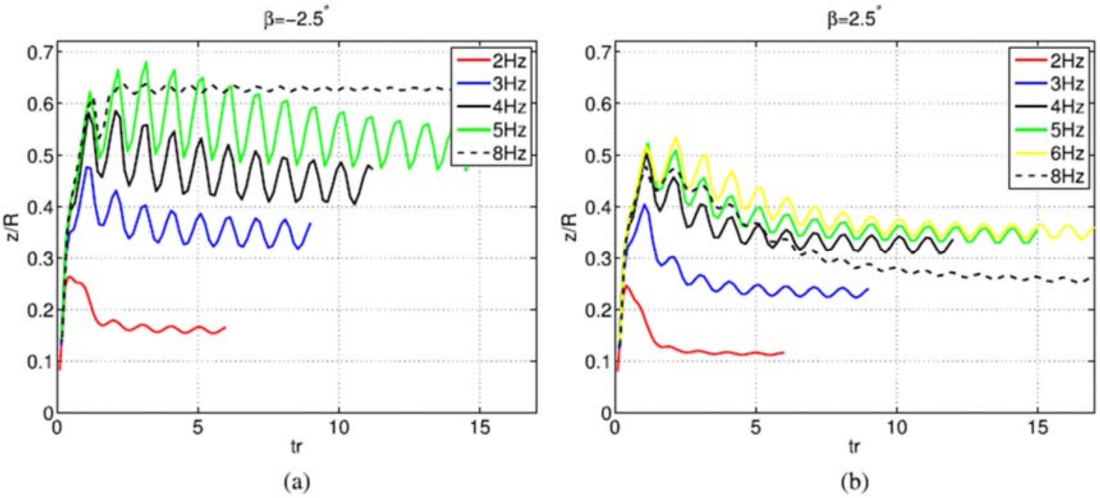

Fig. 8 Total maximum blade deformation variation with the number of revolution for different frequencies: (a) β = 2.5˚ (b) β = 2.5˚

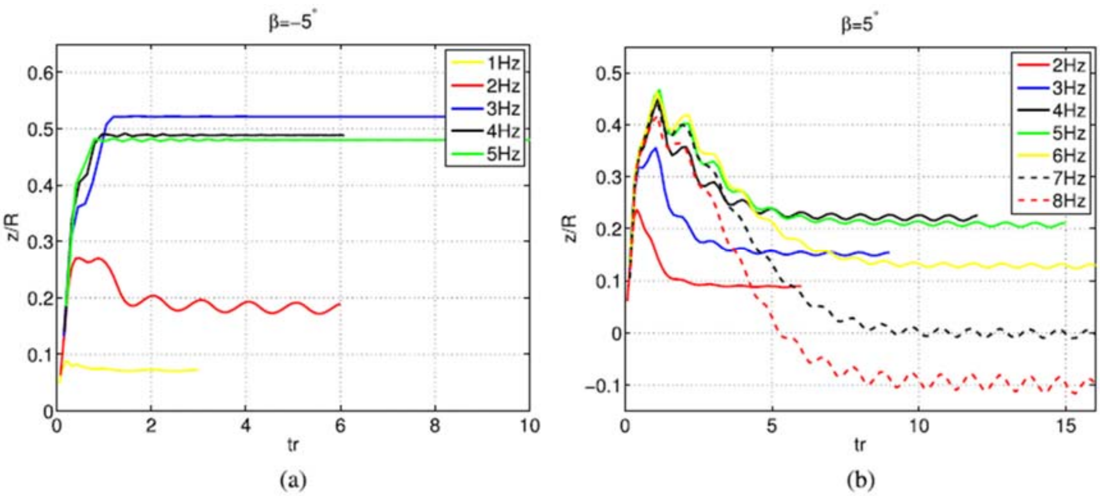

Fig. 9 Total maximum blade deformation variation with the number of revolution for different frequencies: (a) β = 2.5˚ (b) β = 2.5˚

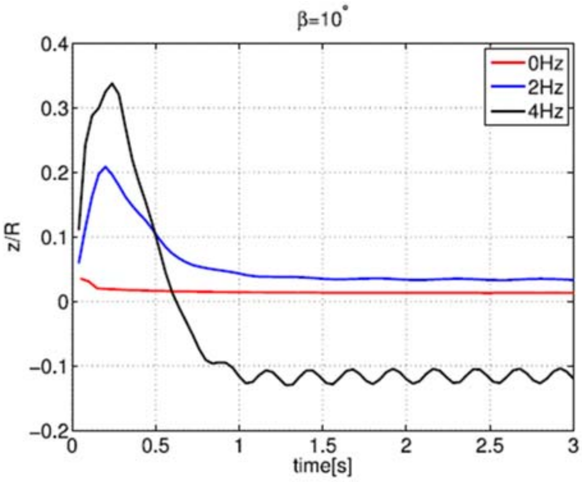

Fig. 10 Total maximum blade deformation variation with time for different frequencies (β = 10˚)

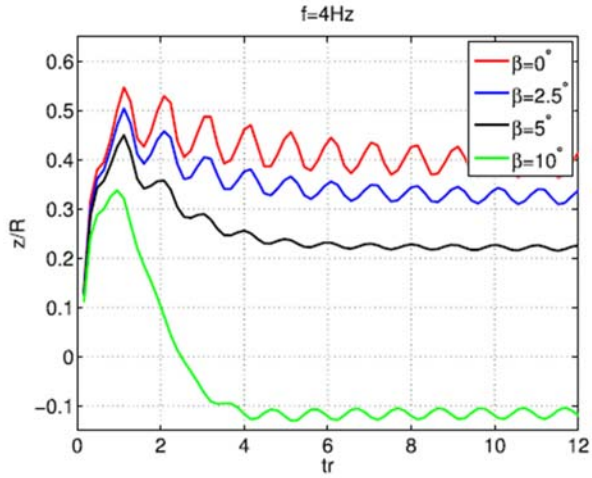

Fig. 11 Blade deformation evolution with time for different pitch angles (f = 4 Hz)

REFERENCES

[1] J. F. Manwell, « Wind Energy Explained: Theory, Design and Application », 2002.
[2] C.-K. Kang, H. Aono, C. E. S. Cesnik and W. Shyy, « Effects of flexibility on the aerodynamic performance of flapping wings », *Journal of Fluid Mechanics*, vol. 689, p. 32-74, déc. 2011, doi: 10.1017/jfm.2011.428.
[3] E. de Langre, A. Gutierrez and J. Cossé, « On the scaling of drag reduction by reconfiguration in plants », *Comptes Rendus Mécanique*, vol. 340, nº 1, p. 35-40, janv. 2012, doi: 10.1016/j.crme.2011.11.005.
[4] F. Gosselin, E. de Langre and B. Machado-Almeida, « Drag reduction of flexible plates by reconfiguration », *Journal of Fluid Mechanics*, vol. 650, p. 319-341, mai 2010, doi: 10.1017/S0022112009993673.
[5] X. Zhang, Z. Wang and W. Li, « Structural optimization of H-type VAWT blade under fluid-structure interaction conditions », *Journal of Vibroengineering*, vol. 23, nº 5, Art. nº 5, 2021, doi: 10.21595/jve.2021.21766.
[6] M. Ali and M. Abid, « Self-similar behaviour of a rotor wake vortex core », *Journal of Fluid Mechanics*, vol. 740, p. R1, févr. 2014, doi: 10.1017/jfm.2013.636.
[7] K. Lee, Z. Huque, R. Kommalapati and S.-E. Han, « Fluid-structure interaction analysis of NREL phase VI wind turbine: Aerodynamic force evaluation and structural analysis using FSI analysis », *Renewable Energy*, vol. 113, nº C, p. 512-531, 2017.
[8] K. Lee, Z. Huque, R. Kommalapati and S.-E. Han, « The Evaluation of Aerodynamic Interaction of Wind Blade Using Fluid Structure Interaction Method », *JOCET*, vol. 3, nº 4, p. 270-275, 2015, doi: 10.7763/JOCET.2015.V3.207.
[9] L. Wang, R. Quant and A. Kolios, « Fluid structure interaction modelling of horizontal-axis wind turbine blades based on CFD and FEA », *Journal of Wind Engineering and Industrial Aerodynamics*, vol. 158, p. 11-25, nov. 2016, doi: 10.1016/j.jweia.2016.09.006.
[10] T. Bano, F. Hegner, M. Heinrich and R. Schwarze, « Investigation of Fluid-Structure Interaction Induced Bending for Elastic Flaps in a Cross Flow », *Applied Sciences*, vol. 10, nº 18, Art. nº 18, jan. 2020, doi: 10.3390/app10186177.
[11] D. Sederstrom, « Methods and Implementation of Fluid-Structure Interaction Modeling into an Industry-Accepted Design Tool », *Electronic Theses and Dissertations*, jan. 2016, (On line) Disponible sur: https://digitalcommons.du.edu/etd/1197